energies

MDPI

Article

A Practical Model for Gas–Water Two-Phase Flow and Fracture Parameter Estimation in Shale

Pin Jia [1,2,*], Langyu Niu [1,2], Yang Li [1,2] and Haoran Feng [1,2]

[1] State Key Laboratory of Petroleum Resources and Prospecting, China University of Petroleum (Beijing), Beijing 102249, China
[2] College of Petroleum Engineering, China University of Petroleum (Beijing), Beijing 102249, China
* Correspondence: jiapin1990@163.com

Abstract: The gas flow in shale reservoirs is controlled by gas desorption diffusion and multiple flow mechanisms in the shale matrix. The treatment of hydraulic fracturing injects a large amount of fracturing fluids into shale reservoirs, and the fracturing fluids can only be recovered by 30~70%. The remaining fracturing fluid invades the reservoir in the form of a water invasion layer. In this paper, by introducing the concept of a water invasion layer, the hydraulic fracture network is di-vided into three zones: major fracture, water invasion layer and stimulated reservoir volume (SRV). The mathematical model considering gas desorption, the water invasion layer and gas–water two-phase flow in a major fracture is established in the Laplace domain, and the semi-analytical solution method is developed. The new model is validated by a commercial simulator. A field case from WY shale gas reservoir in southwestern China is used to verify the utility of the model. Several key parameters of major fracture and SRV are interpreted. The gas–water two-phase flow model established in this paper provides theoretical guidance for fracturing effectiveness evaluation and an efficient development strategy of shale gas reservoirs.

Keywords: shale gas; gas–water two-phase; fluid model; water invasion layer; parameter estimation of fracture network

check for updates

Citation: Jia, P.; Niu, L.; Li, Y.; Feng, H. A Practical Model for Gas–Water Two-Phase Flow and Fracture Parameter Estimation in Shale. *Energies* **2023**, *16*, 5140. https://doi.org/10.3390/en16135140

Academic Editor: Reza Rezaee

Received: 11 February 2023
Revised: 13 April 2023
Accepted: 14 April 2023
Published: 3 July 2023

Copyright: © 2023 by the authors. Licensee MDPI, Basel, Switzerland. This article is an open access article distributed under the terms and conditions of the Creative Commons Attribution (CC BY) license (https://creativecommons.org/licenses/by/4.0/).

1. Introduction

Due to the large amount of fracturing fluids injected, the hydraulic fracture networks and the surrounding matrix in the shale reservoir are complex. After a shut-in period, the fracturing fluids will create a water blockage in the shale matrix near fractures, which essentially is formation damage with a lower permeability. In this paper, the fracture network and matrix in shale gas reservoirs are classified into three systems: stimulated reservoir volume (SRV), water invasion layer and hydraulic fracture. The current gas–water two-phase flow model does not consider the influence of the water invasion layer on gas well production. Thus, it is difficult to accurately interpret the parameters of a complex fracture network and evaluate the fracturing effectiveness.

In 1998, Wattenbarger et al. [1] proposed a linear flow model for production dynamic analysis of tight gas wells. In 2010, Bello and Wattenbarger [2] developed a cylindrical dual-porosity model, and this model proved to be useful for productivity analysis of fractured horizontal wells, and the flow regimes during production were analyzed using this model. In 2011, Al-Ahmadi and Wattenbarger [3] considered secondary fractures of the reservoir based on the dual-porosity model, and the SRV was therefore considered as a tri-porosity model. In the model, the quasi-steady and unsteady flow transfer between matrix-secondary fracture and primary fracture are considered. The analytical solution of the model is obtained in Laplace space, and the flow regimes were obtained. The model shows the strong ability to interpret the complex fracture network in shale reservoirs. In 2011, Brown et al. [4] established a model with the assumption that the fluid from the outer zone was supplied to the inner zone, and then flowed into the main fracture from

the inner zone, and finally into the wellbore. A classical trilinear flow model was set up, and several local approximate solutions of the model were obtained, which were suitable for linear and bilinear flow stages. At present, this model has been widely used in the production performance analysis of unconventional oil and gas wells. Then, Stalgorova and Mattar [5] divided the fractured horizontal well model into five regions by further considering the unstimulated regions between the various levels of fracture and gave the solution in the Laplace domain. Ai [6] established a prediction model for shale gas well productivity considering the contribution of unstimulated reservoir volume (unSRV) to the productivity. From the literatures, the current studies rarely consider the influence of water invasion layer in the modeling of fractured horizontal wells and the estimation of the parameters of fracture network in shale reservoirs. AlQuaimi [7] proposed a new capillary-number definition for fractures that incorporates geometrical characterization of the fracture, dependent on the force balance on a trapped ganglion.

In this paper, the SRV, water invasion layer and hydraulic fracture are finely divided. The influence of the water invasion layer on production is considered in reservoir modeling. A new model considering gas adsorption of shale matrix, water invasion layer and gas–water two-phase flow in hydraulic fractures is established and solved semi-analytically in this paper. Additionally, a fitting method of production data is proposed for the estimation of fracture network parameters of shale reservoirs.

2. Mathematical Model for Gas-Water Two-Phase Flow

2.1. Physical Model and Assumptions

In Figure 1, the white zone is the hydraulic fracture, the blue zone is the water invasion layer and the dark gray zone is the SRV, also known as the inner zone. The light gray zone is the unSRV, also known as the outer zone. Since we focus on the gas–water two-phase flow period at the early stage of gas well production, the linear flow in the unSRV (outer zone) has little influence on the production. The flow in the unSRV is not considered, as shown in Figure 1.

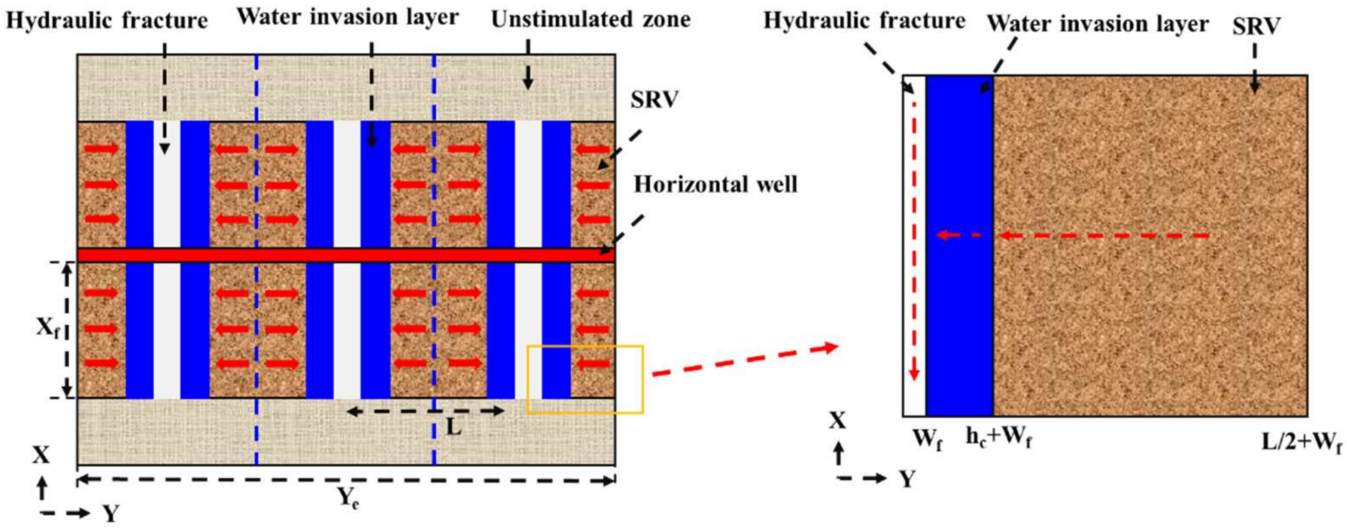


Figure 1. The schematic diagram of physical model.

With the production, the gas in the SRV flows linearly from the matrix to the water invasion layer, then reaches the hydraulic fracture, and finally flows into the wellbore. The following assumptions are made:

(1) The reservoir is of equal thickness, homogeneous and closed. The horizontal well maintains constant pressure production.
(2) Gas flow is considered to be single-phase in the SRV, and gas–water two-phase flow is considered in the water invasion layer and hydraulic fracture.

(3) The effects of gas desorption and slippage are considered in the shale matrix, and the stress sensitivity of hydraulic fracture is considered.

2.2. Single-Phase Gas Flow in Stimulated Reservoir

As shown in Figure 2, both free gas and adsorbed gas exist in the shale matrix. As the reservoir pressure drops, the free gas and adsorbed gas in the matrix expand to provide gas.

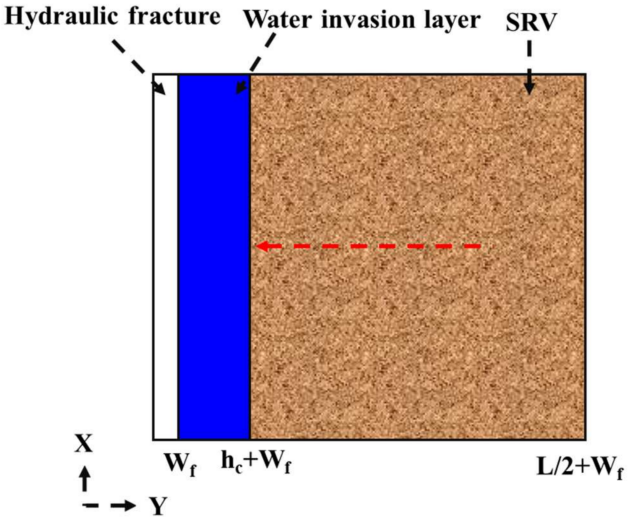


Figure 2. Single-phase gas flow in the SRV.

The single-phase gas flow equation can be written as follows:

$$\frac{\partial}{\partial y}(-\rho_{sc} v_m) = 0.0864[\frac{\partial(\rho\phi_m)}{\partial t} + \frac{\partial V}{\partial t}] \tag{1}$$

where, ρ_{sc} is the gas density in standard condition, kg/m^3; ϕ_m is matrix porosity, dimensionless; t is time, d; v_m is the gas flow velocity, m/d; and V is the adsorption capacity of the SRV, m^3. The second term on the right side of the equation represents the mass of gas desorbed from the surface of shale matrix per unit volume per unit time.

According to the Langmuir equation of gas adsorption and desorption [8], the amount of desorption at any point in the formation is closely related to the matrix pressure at that point. Thus, the gas isothermal adsorption equation is introduced as follows:

$$V = \rho_{sc} \frac{V_L p_m}{p_L + p_m} \tag{2}$$

where, p_m is the matrix pressure, MPa; V is adsorption capacity, m^3; V_L is the Langmuir volume, m^3/m^3; p_L is Langmuir pressure, MPa; and ρ_{sc} is the gas density in standard condition, kg/m^3.

By introducing the pseudo-pressure:

$$\psi_m(p_m) = 2\int_{p_i}^{p_m} \frac{p}{\mu_g z} dp \tag{3}$$

The gas flow equation of the SRV is expressed as:

$$\frac{\partial^2 \psi_m}{\partial y^2} = 0.0864 \frac{\phi_m \mu_g(p_m) c_{tm}(p_m)}{k_m} \frac{\partial \psi_m}{\partial t} \tag{4}$$

Further, for the nonlinear term on the right side of the equation, pseudo-time is used, which is defined as:

$$t_a = \int_0^t \frac{\mu_{gi} c_{tmi}}{\mu_g(\overline{p}_m) c_{tm}(\overline{p}_m)} dt \tag{5}$$

Thus, the single-phase gas flow equation in the SRV is rearranged by using the pseudo-pressure and pseudo-time, and the gas flow model in the SRV can be obtained as follows:

$$\begin{cases} \frac{\partial^2 \psi_m}{\partial y^2} = \frac{\mu_{gi}(\phi c_t)_{mi}}{0.0864 k_m} \frac{\partial \psi_m}{\partial t_a} \\ \psi_m(y,t)|_{t_a=0} = \psi_i \\ \left.\frac{\partial \psi_m(y,t_a)}{\partial y}\right|_{y=L_F/2} = 0 \end{cases} \tag{6}$$

The inner boundary of the SRV is coupled with the water invasion layer system, and the pressure and flow rate on the inner boundary and the water invasion layer boundary should be equal, respectively:

$$\psi_m|_{y=h_c+w_F/2} = \psi_c|_{y=h_c+w_F/2} \tag{7}$$

2.3. Gas-Water Two-Phase Flow in Water Invasion Layer

After hydraulic fracturing, the water (fracturing fluid) invade into the shale matrix through mass transfer from the hydraulic fracture. As shown in Figure 3, This fluid is movable water during the flowback period, and gas–water two-phase flow occurs in this zone.

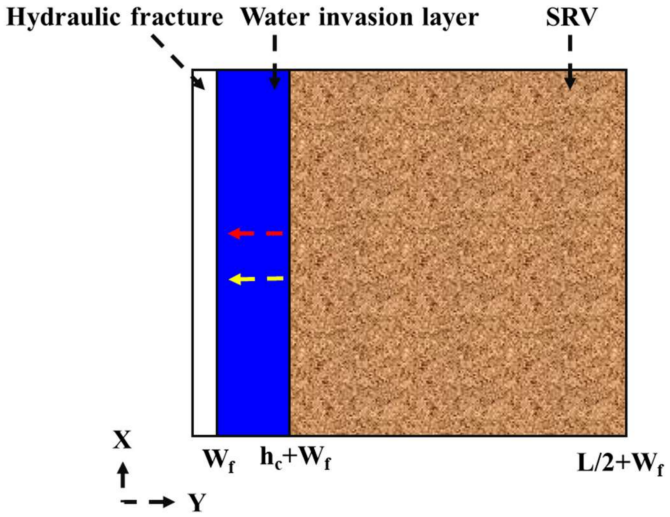


Figure 3. Gas–water two-phase fluid in water invasion layer.

The flow equation of gas phase in the water invasion layer is similar to the flow equation of gas phase in the SRV. The gas flow equation also uses pseudo-pressure and pseudo-time, and can be obtained as follows:

$$\begin{cases} \frac{\partial^2 \psi_c}{\partial y^2} = \frac{\mu_{gi}(\phi_c c_t)_{ci}}{0.0864 k_c \hat{k}_{crg}} \frac{\partial \psi_c}{\partial t_a} \\ \psi_c(y,t_a)|_{t_a=0} = \psi_i \end{cases} \tag{8}$$

where, $\hat{k}_{crg}$ is the relative permeability of the gas phase in the water invasion layer, the relative permeability is a function of gas saturation. In this paper, time is discretized into several time steps, and in each time step, an average saturation is taken, which can be treated as a constant in a single time step. ϕ_c is the porosity of water invasion layer,

dimensionless; μ_g is gas viscosity, mPa·s; ψ_c is the pseudo-pressure of water invasion layer, $(MPa)^2/(mPa, s)$; and c_{tc} is the total compressibility of water invasion layer system, MPa^{-1}.

The outer boundary of the water invasion layer is coupled with the system flow model of the SRV, and the coupling condition is as follows:

$$k_m \frac{\partial \psi_m}{\partial y}\bigg|_{y=h_c+w_F/2} = k_c \frac{\partial \psi_c}{\partial y}\bigg|_{y=h_c+w_F/2} \tag{9}$$

The inner boundary is coupled to the boundary of the hydraulic fracture, so the pressure at the interface of these two zones should be equal, i.e.,

$$\psi_c(y, t_a)|_{y=w_F/2} = \psi_F \tag{10}$$

The water flow equation can be obtained as follows:

$$\begin{cases} \frac{\partial^2 p_c}{\partial y^2} = \frac{1}{0.0864} \frac{\phi_c c_{tc}^* \mu_w}{k_c \hat{k}_{crw}} \frac{\partial p_c}{\partial t} \\ p_c(y, t)|_{t=0} = p_i \\ \frac{\partial p_c}{\partial y}\Big|_{y=h_c+w_F/2} = 0 \end{cases} \tag{11}$$

Due to the coupling between the inner boundary of the water invasion layer and the hydraulic fracture system, the pressure at the interface of these two zones should be equal, i.e.,

$$p_c(y, t)|_{y=w_F/2} = p_F \tag{12}$$

2.4. Gas-Water Two-Phase Flow in Hydraulic Fracture

Similar to the water invasion layer, the hydraulic fracture is filled with fracturing fluid after fracturing stimulation, and gas–water two-phase flow occurs during flowback. As shown in Figure 4, The gas and water continuously supply the hydraulic fracture through the water invasion layer.

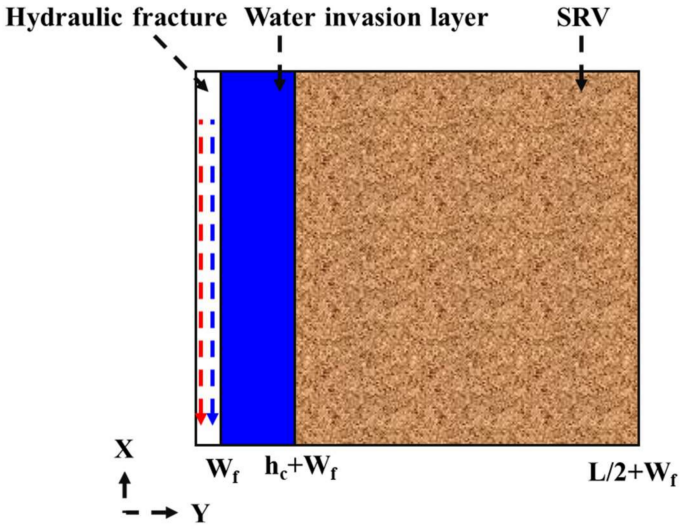


Figure 4. Gas–water two-phase flow in the major fracture.

The governing equation of gas flow in the hydraulic fracture can be expressed as follows:

$$\frac{\partial}{\partial x}(\rho_g v_F) + \rho_g q_{cg} = 0.0864 \frac{\partial(\rho_g \phi_F)}{\partial t} \tag{13}$$

where, v_{Fg} is the gas-phase fluid velocity of the hydraulic fracture, m/d; ϕ_F is hydraulic fracture porosity, dimensionless; k_F is permeability of hydraulic fractures, mD; p_F is the

hydraulic fracture pressure, MPa; and q_{cg} is the gas flow rate into the hydraulic fracture per unit volume of the water invasion layer system per unit time (unit m)^3/d.

Then, the equation of gas flow in the hydraulic fracture is:

$$\begin{cases} \frac{\partial^2 \psi_F}{\partial x^2} = 0.0864\left[\frac{\mu_{gi}(\phi c_t)_{Fi}}{k_F \hat{k}_{Frg}} \frac{\partial \psi_F}{\partial t_a} - \frac{2k_c \hat{k}_{crg}}{w_F k_F \hat{k}_{Frg}} \frac{\partial \psi_c}{\partial y}\Big|_{y=w_F/2}\right] \\ \psi_F(x,t_a)|_{t_a=0} = \psi_i \\ \frac{\partial \psi_F(x,t_a)}{\partial x}\Big|_{x=x_F} = 0 \\ \psi_F(x,t_a)|_{x=0} = \psi_w \end{cases} \tag{14}$$

The water phase flow equation in the hydraulic fracture system is:

$$\begin{cases} \frac{\partial^2 p_F}{\partial x^2} = 0.0864\left[\frac{\phi_F c_{tF}^* \mu_w}{k_F \hat{k}_{Frw}} \frac{\partial p_F}{\partial t} - \frac{2k_c \hat{k}_{crw}}{w_F k_F \hat{k}_{Frw}} \frac{\partial p_c}{\partial y}\Big|_{y=w_F/2}\right] \\ p_F(x,t)|_{t=0} = p_i \\ \frac{\partial p_F(x,t)}{\partial x}\Big|_{x=x_F} = 0 \\ p_F(x,t)|_{x=0} = p_w \end{cases} \tag{15}$$

2.5. Dimensionless Model and Lapalce Transform

For the convenience of derivation, the mathematical model adopts a dimensionless form. The definition of dimensionless is shown in Table 1:

Table 1. Dimensionless parameter definition.

Dimensionless Parameters	Define
Dimensionless x	$x_D = \frac{x}{L_r}$
Dimensionless time	$t_D = \frac{\eta_r}{L_r^2} t$
Dimensionless permeability	$k_D = \frac{k}{k_r}$
Dimensionless y	$y_D = \frac{y}{L_r}$
Dimensionless pseudo-time	$t_{aD} = \frac{\eta_r}{L_r^2} t_a$
Dimensionless hydraulic fracture conductivity	$C_{FD} = \frac{w_F k_F}{k_c L_r} = \frac{k_{FD} w_{FD}}{k_{cD}}$

3. Solution of Gas–Water Two-Phase Flow Model

Due to the nonlinearity of the gas and water flow equations, the solution of the model is solved semi-analytically. Time is discretized, and in a single step, the average saturation is treated as a constant value. Additionally, it can have an analytic solution and be solved by Stehfest [9] to obtain the solution of the model in real space. Then, the average saturation at the next time step is calculated by using the mass balance equation of gas and water flow. Finally, the gas and water production are predicted successively, forming a semi-analytical solution method for the gas–water two-phase flow model.

3.1. Solution of Gas Flow Equation

In this paper, the solution of the model is obtained by using the Laplace transform. The dimensionless Laplace transform of each equation is taken and then can be derived. The solution of gas production is obtained as follows.

$$\overline{q}_{gD} = \frac{\hat{k}_{Frg} k_{FD} w_{FD}}{\pi} \frac{1 - S_c}{s} \sqrt{c_4(s)} \tanh\left(\sqrt{c_4(s)} \cdot x_{FD}\right) \tag{16}$$

It should be noted that the gas production equation derived from analytical solution is in Laplace space, while the solution in real space needs to be obtained by a Stehfest numerical inversion algorithm. In addition, the Laplace transform is about dimensionless pseudo-time, while the Laplace transform of the water phase equation is about dimensionless time, so these two equations must be distinguished. Appendix B provides the detail derivation of the gas flow model and the constant in Equation (16) is expressed as:

$$\begin{cases} c_1(s) = \frac{k_m}{k_c}\frac{\sqrt{s/\eta_{mD}}}{\sqrt{s/(\hat{k}_{crg}\eta_{cD})}}\tanh\left[\sqrt{\frac{s}{\eta_{mD}}}(h_{cD}+w_{FD}/2-L_{FD}/2)\right] \\ c_2(s) = \cosh\left[\sqrt{\frac{s}{\hat{k}_{crg}\eta_{cD}}}(-h_{cD})\right] + c_1(s)\sinh\left[\sqrt{\frac{s}{\hat{k}_{crg}\eta_{cD}}}(-h_{cD})\right] \\ c_3(s) = \sqrt{\frac{s}{\hat{k}_{crg}\eta_{cD}}}\frac{\sinh\left[\sqrt{\frac{s}{\hat{k}_{crg}\eta_{cD}}}(-h_{cD})\right]+c_1(s)\cosh\left[\sqrt{\frac{s}{\hat{k}_{crg}\eta_{cD}}}(-h_{cD})\right]}{c_2(s)} \\ c_4(s) = \frac{s}{\hat{k}_{Frg}\eta_{FD}} - \frac{2\hat{k}_{crg}}{C_{FD}\hat{k}_{Frg}}c_3(s) \\ \overline{q}_{gD} = \frac{\hat{k}_{Frg}k_{FD}w_{FD}}{\pi}\frac{1-S_c}{s}\sqrt{c_4(s)}\tanh\left(\sqrt{c_4(s)}\cdot x_{FD}\right) \end{cases} \tag{17}$$

3.2. Solution of Water Flow Equation

Similar to the derivation of the gas flow equation in the above section, we also adopt the Laplace transform to obtain the water flow solution of the model.

The solution of water phase production is expressed as follows:

$$\overline{q}_{wD} = -\frac{\hat{k}_{Frw}k_{FD}w_{FD}}{\pi}\frac{\partial\overline{p}_{FD}}{\partial x_D}\bigg|_{x_D=0} = \frac{\hat{k}_{Frw}k_{FD}w_{FD}}{\pi}\frac{1-S_c}{s}\sqrt{d_2(s)}\tanh\left(\sqrt{d_2(s)}\cdot x_{FD}\right) \tag{18}$$

Appendix C provides the detail derivation of the gas flow model and the constant in Equation (17) is expressed as:

$$\begin{cases} d_1(s) = \sqrt{\frac{s}{\hat{k}_{crw}\eta_{cwD}}}\tanh\left[\sqrt{\frac{s}{\hat{k}_{crw}\eta_{cwD}}}(-h_{cD})\right] \\ d_2(s) = \frac{s}{\hat{k}_{Frw}\eta_{FwD}} - \frac{2\hat{k}_{crw}}{C_{FD}\hat{k}_{Frw}}d_1(s) \\ \overline{q}_{wD} = -\frac{\hat{k}_{Frw}k_{FD}w_{FD}}{\pi}\frac{1-S_c}{s}\frac{\partial\overline{p}_{FD}}{\partial x_D}\Big|_{x_D=0} = \frac{\hat{k}_{Frw}k_{FD}w_{FD}}{\pi}\frac{1-S_c}{s}\sqrt{d_2(s)}\tanh\left(\sqrt{d_2(s)}\cdot x_{FD}\right) \end{cases} \tag{19}$$

3.3. Solution Procedure of the Model

To solve the above equations, we must rely on gas and water mass balance equations for calculating the average pressure of the SRV system and the average saturation of the fracture system, and then update the saturation-dependent and pressure-dependent parameter in Equations (16) and (18). The mass balance equation of water in the fracture and the water invasion layer are given as follows:

$$W_p = V_{pFc}\left(\frac{S_{wi}}{B_{wi}} - \frac{\hat{S}_w}{B_w}\right) \tag{20}$$

$$\hat{S}_w = S_{wi} - \frac{W_p}{V_{pFc}} \tag{21}$$

The gas mass balance equation is:

$$\begin{aligned} W_g &= V_{pm}S_{mgi}\left(\frac{1}{B_{gi}}-\frac{1}{B_g}\right)+V_{pm}\left(\frac{V_L p_i}{p_L+p_i}-\frac{V_L \hat{p}}{p_L+\hat{p}}\right) \\ &+V_{pFc}\left(\frac{1-S_{wi}}{B_{gi}}-\frac{1-\hat{S}_w}{B_g}\right)+V_{pFc}\left(\frac{V_L p_i}{p_L+p_i}-\frac{V_L \hat{p}}{p_L+\hat{p}}\right) \end{aligned} \quad (22)$$

In a shale gas reservoir, the fracture system provides a high-conductivity gas flow channel, but the compressibility of the fracture system is small. Hence, during flowback, the average pressure of the SRV system is much higher than that of the fracture system. Additionally, the average pressure of the fracture system is approximately equal to the bottom-hole flowing pressure, and the average pressure of the matrix system is close to that of the reservoir. Therefore, for the calculation of water phase flow, the unified average water saturation is used to calculate the fracture and water invasion layer, while the average pressure of the fracture system is calculated by the fracture pressure solution, and the average pressure of the water invasion layer system is calculated by the water invasion layer pressure solution. For the gas phase, the gas saturation is calculated based on the average water saturation, and the average pressure is calculated using the gas-phase mass balance equation. The model calculation process is shown in Figure 5.

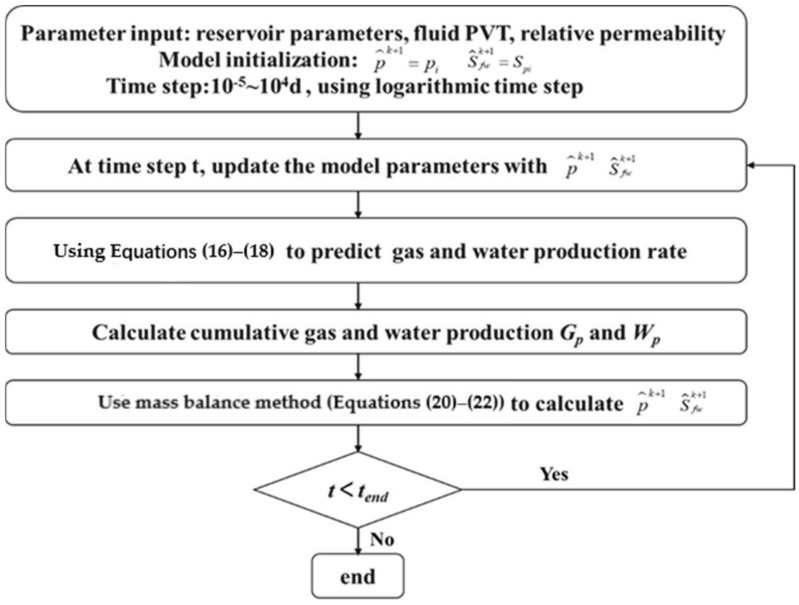


Figure 5. Semi-analytical solution flow of gas–water two-phase flow model.

3.4. Model Validation

In order to validate the accuracy of the gas–water flow model and the semi-analytical solution method, this paper uses a commercial reservoir numerical simulator to establish a set of discrete fracture systems (as shown in Figure 6). The gas–water production results of numerical simulation are compared with that of the flow model.

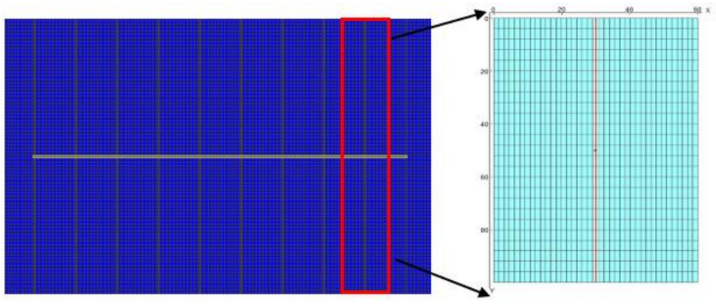


Figure 6. Schematic diagram of the numerical simulation grid.

The grid systems of the numerical simulation is 430 × 25 × 1, and the total number of grids is 10,750. In order to accurately represent the fracture width, the mesh around the fracture is refined. The mesh size near the fracture is 0.045 m and 0.01 m, and the width of the fracture is represented by the grids with the width of 0.01 m. The basic parameters used are shown in Table 2.

Table 2. Parameters used for model comparison.

Parameter	The Numerical
Fracture porosity, %	45
Crack compression coefficient, MPa^{-1}	1.0×10^{-3}
Fracture permeability, mD	1000
Crack half-length, M	100
Initial fracture water saturation, %	100
Matrix compression coefficient, MPa^{-1}	1.0×10^{-4}
Width of water invasion layer, m	2
Matrix permeability, mD	1.0×10^{-4}
Effective reservoir thickness, m	10
Initial gas saturation of the matrix, %	70
Initial crack pressure, MPa	29.5
Matrix porosity, %	6.4
Bottom hole flow pressure, MPa	2
Permeability of water invasion layer, mD	5.0×10^{-5}

The comparison results are shown in Figures 7 and 8. It can be seen that the water and gas production predicted by the two methods are in good agreement. Therefore, the established gas–water flow model is correct and can accurately characterize the gas–water flow process of shale reservoirs, and the model is relatively reliable.

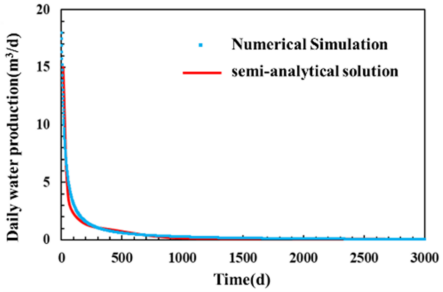


Figure 7. Daily water flow curves.

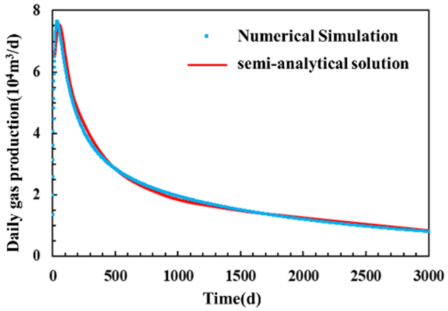


Figure 8. Daily gas volume.

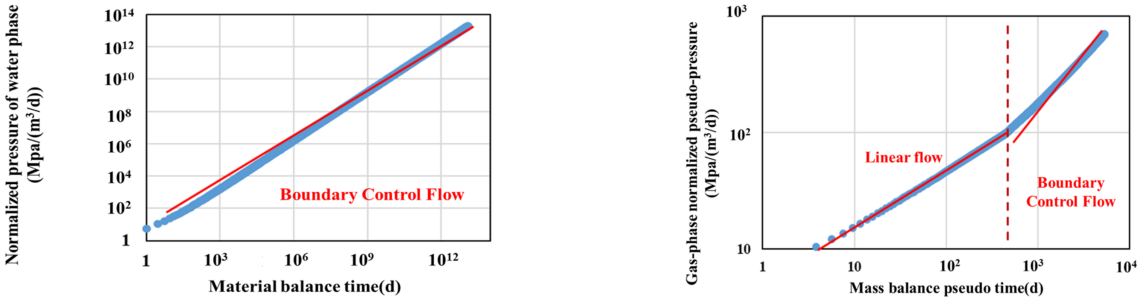
4. Interpretation of Fracture Network Parameters

4.1. Flow Regimes of Gas-Water

There are usually two modes of production in shale gas reservoirs. The first mode shows gas–water two-phase flow in the early flowback period, while the second mode usually shows a single-phase fracturing fluid flowback period with several days. The gas in the matrix enters the fracture and then shows a two-phase flow.

4.1.1. Flow Regimes of Gas-Water in the First Mode

Figure 9 shows the flow characteristics of the first mode of gas–water production.



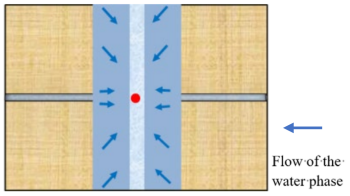
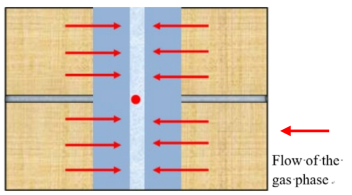
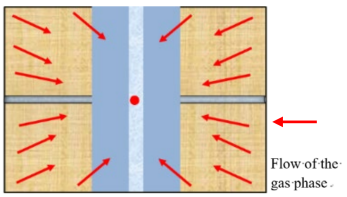
(**a**) (**b**)

Figure 9. Typical gas–water flow regimes in the first type of production mode. (**a**) Typical flow characteristics of water phase, and (**b**) typical flow characteristics of gas phase.

(1) Water boundary dominated flow. Because the fracturing fluid mainly occurs in the hydraulic fracture, water will drain very fast and then show the boundary dominated flow, until the water production rate is nearly zero. On the plot of rate normalized pressure and mass balance time, the curve shows a unit slope straight line.
(2) Gas linear flow. This flow regime occurs at almost the same time with a water boundary dominated flow, and is the first flow stage of the gas phase. At this time, the gas in the matrix flows to the fracture in a direction perpendicular to the fracture surface, which appears as straight with one-half slope on the typical curve.
(3) Gas boundary dominated flow. With the production, the gas pressure drop reaches the closed boundary and forms the boundary dominated flow, which is represented as a straight line with a unit slope on the typical curve shown.

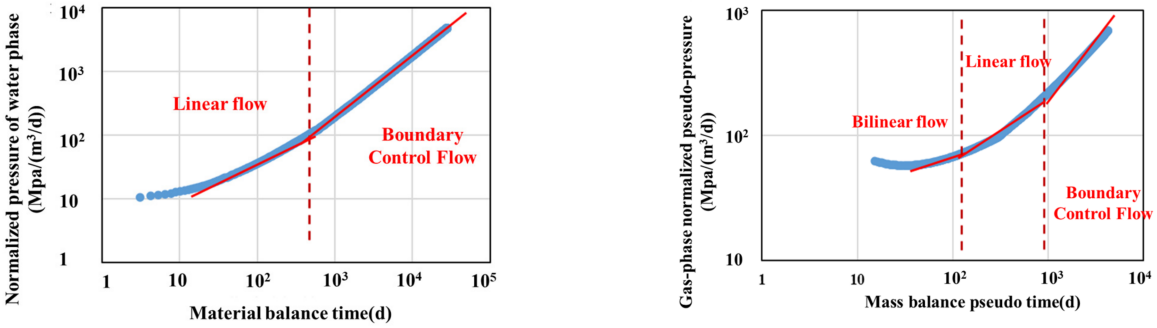
The description and schematic diagram of each flow regimes are summarized in Table 3.

Table 3. Description of gas–water flow in the first type of production mode.

Flow Regime	Description	Schematic Diagram
Water boundary dominated flow	The fracturing fluid flows along the hydraulic fracture into the wellbore, and the water exhibits depletion in the fracture	
Gas linear flow	Gas in matrix flows into the fracture in a direction perpendicular to the fracture surface, and the gas dominates the fracture flow	
Gas boundary dominated flow	After the gas pressure drop boundary reaches the closed boundary, the closed boundary control flow is formed	

4.1.2. Flow Regimes of Gas-Water in the Second Mode

Figure 10 describes the flow characteristics in each stage of the second type of gas–water production.



(**a**) (**b**)

Figure 10. Gas–water flow stage in the second type of production dynamic mode. (**a**) Typical flow characteristics of water phase, and (**b**) typical flow characteristics of gas phase.

(1) Water linear flow. Since fracturing fluid exists in both the hydraulic fracture and the invasion layer, linear flow of the water phase will occur when the pressure drop in the water invasion layer after the flowback starts. The typical curve shows a straight line with a unit slope.
(2) Water boundary dominated flow. Due to the fracturing fluid mainly occurs in the hydraulic fracture, water will drain very fast and then show the boundary dominated flow, until the water production rate is nearly zero. On the plot of rate normalized pressure and mass balance time, the curve shows a unit slope straight line.
(3) Gas bilinear flow. Gas phase flow into the hydraulic fracture soon after the flowback starts and forms bilinear flow with the pressure drop system formed by the water invasion layer and shale matrix, which is represented as a straight line with a quarter-slope.
(4) Gas linear flow. This flow regime occurs at almost the same time with water boundary dominated flow, and is the first flow stage of the gas phase. At this time, the gas in the matrix flows to the fracture in a direction perpendicular to the fracture surface, which appears as a straight line with one-half slope on the typical curve.
(5) Gas boundary dominated flow. With the production, the gas pressure drop reaches the closed boundary and forms the boundary dominated flow, which is represented as a straight line with a unit slope on the typical curve shown.

The description and schematic diagram of each flow regime are summarized in Table 4.

Table 4. Description of gas–water flow in the second type of production mode.

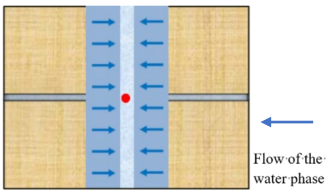
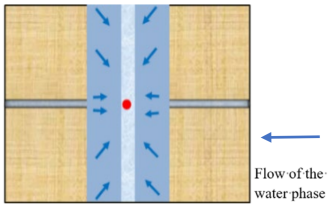
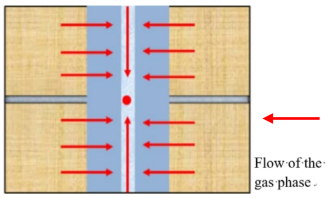
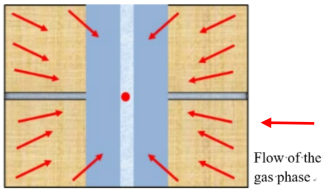
Liquid Phase	Flow Phase Description	Schematic Diagram
Water linear flow	The water fluid flows linearly to the wellbore along the invasion layer. This stage occurs at the beginning of the flowback.	

Table 4. *Cont.*

Liquid Phase	Flow Phase Description	Schematic Diagram
Water boundary dominated flow	The fracturing fluid flows along the hydraulic fracture into the wellbore, and the water exhibits depletion in the fracture	
Gas linear flow	Gas in matrix flows into the fracture in a direction perpendicular to the fracture surface, and the gas dominates the fracture flow	
Gas boundary dominated flow	After the gas pressure drop boundary reaches the closed boundary, the closed boundary control flow is formed	

4.2. Interpretation Procedure Fracture Network Parameters

The interpretation of the fracture network is to fit the dynamic data of gas and water production using the new model. Based on the new model, this section proposes a fitting method for the problem of variable flow pressure production. Thus, Equation (23) can be used to convert the production under constant bottomhole flow pressure into that under variable flow pressure.

$$q(t) = \sum_{k=1}^{n} \left[\left(\Delta\psi_{wf,k} - \Delta\psi_{wf,k-1} \right) \cdot q_{cp}(t - t_{k-1}) \right] \tag{23}$$

where, $\left(\Delta\psi_{wf,k} - \Delta\psi_{wf,k-1} \right)$ is the pressure history and $q_{cp}(t - t_{k-1})$ is the constant pressure solution. Thus, the main steps are as follows:

(1) Initial parameter input: set the initial value of the parameters of fracture network, including the fracture half-length, the fracture permeability, the thickness of the water invasion layer, the permeability of the water invasion layer, the width and permeability of the SRV. Additionally, set $\overline{p} = p_1, \overline{S}_g = S_{g1}$.
(2) Take days as the time step, and update the parameters of the gas–water flow model with the $\overline{p}, \overline{S}_g, \eta, \alpha, \beta, \chi$.
(3) Constant pressure solution: gas and water production are calculated by using the gas–water two-phase flow model.
(4) Variable pressure solution: Equation (23) is used to obtain the gas production and water production under variable bottomhole flow pressure.
(5) Calculation of average pressure and saturation: the average pressure and saturation calculated by the material balance method are then substituted into step (2) for recurrent calculation.
(6) If the fitting error between simulated and actual data meets the criterion of convergence, the calculation is finished. Otherwise, update the fitting parameters and repeat the above steps.

The detailed flow chart is shown in Figure 11.

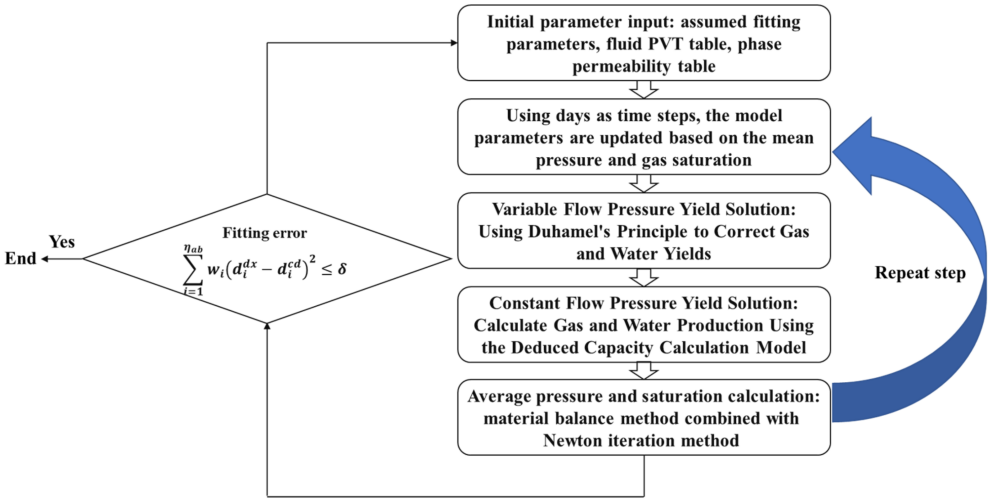
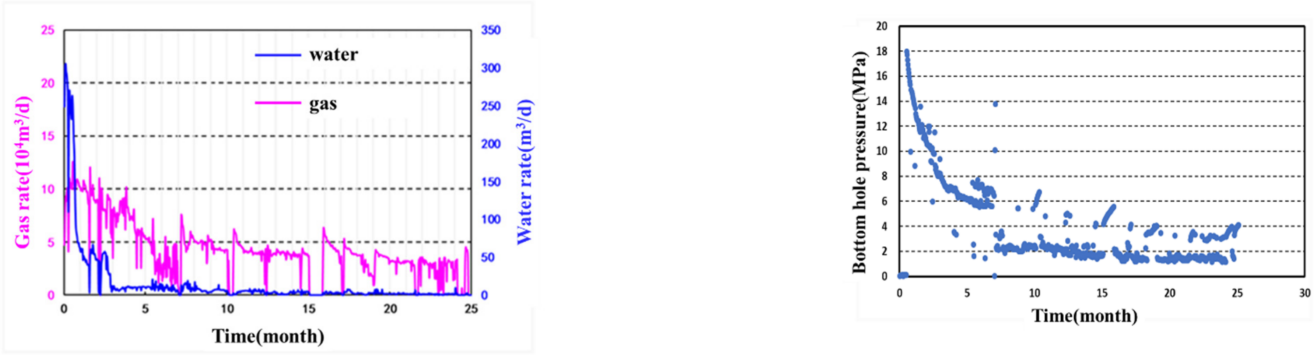


Figure 11. The flow chart of interpretation of the fracture network parameters.

4.3. Field Exmaple

4.3.1. Well A

The gas–water production and bottomhole pressure of the well are shown in Figure 12.



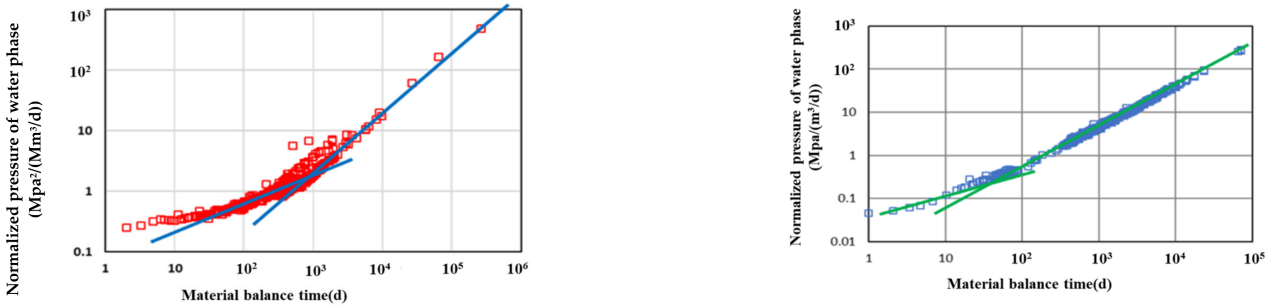
(**a**) (**b**)

Figure 12. Gas–water production and pressure data of well A. (**a**) Gas–water production rate, and (**b**) Bottomhole flow pressure.

The reservoir parameters, fluid parameters and fracturing parameters are shown in Table 5. Analysis of gas–water two-phase flow regime of well A. are as shown in Figure 13.

Table 5. Values of basic parameters of well A.

Parameter	Value
Initial pressure, MPa	29.65
Initial gas saturation, decimal	0.6
Reservoir temperature, K	358.1
Reservoir thickness, m	15
Langmuir volume	2.86
Langmuir pressure, MPa	9.18
Horizontal well length, m	1441
Number of fractures	25
Matrix porosity	0.064
Matrix Compressibility, MPa^{-1}	8×10^{-5}
Fracture Compressibility, MPa^{-1}	8×10^{-5}
Fracture width, m	0.5×10^{-2}

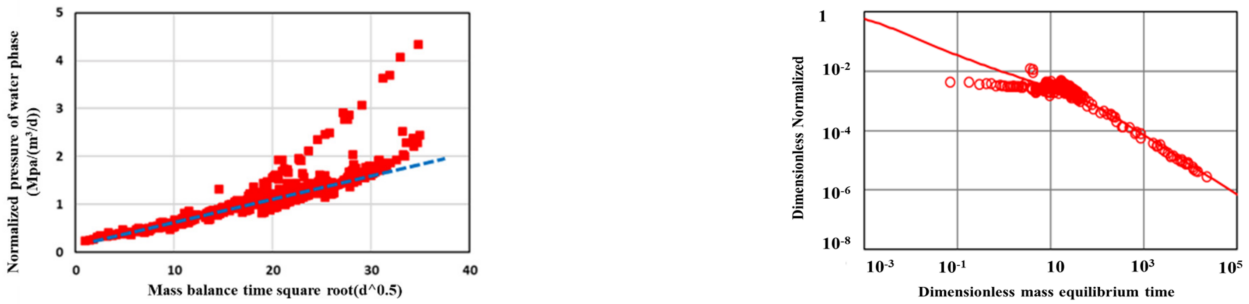


(**a**) (**b**)

Figure 13. Analysis of gas–water two-phase flow regime of well A. (**a**) Gas phase flow regime, and (**b**) water phase flow regime.

In early production, gas exhibits a long linear flow and the gas enters the fracture after 14 months. For the water, it exhibits a fracture linear flow and then the boundary dominated flow, when most fracturing fluid has been discharged. This means that the fracture conductivity is high and the fracture half-length is large.

Based on the results from Figure 14, the total length of the discrete fracture is 4105 m, and the stimulated reservoir volume is 1286 $\times$ 10^4 m^3. The detailed parameters of the fracture network are shown in Table 6.



(**a**) (**b**)

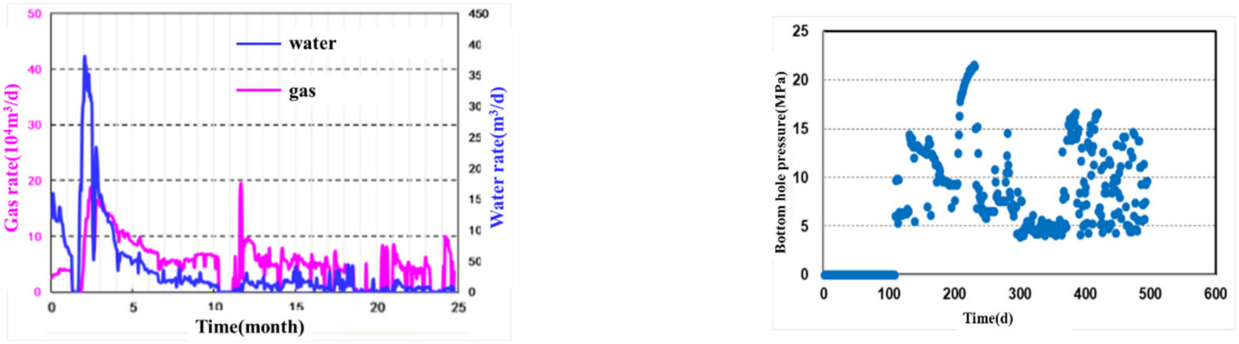
Figure 14. Production decline analysis of gas phase of well B with gas–water two phases. (**a**) Gas phase linear flow analysis, and (**b**) gas production data matching.

Table 6. Interpretation of fracture network parameters of well A.

Interpreted Parameters	Value
Fracture half-length (m)	83.1
Fracture permeability (mD)	865
Thickness of water invasion layer (m)	0.12
Permeability of water invasion (mD)	2.82×10^{-3}
SRV width (m)	46.5
SRV Permeability (mD)	3.87×10^{-3}

4.3.2. Well B

The gas–water production and bottomhole pressure of the well are shown in Figure 15.



(**a**) (**b**)

Figure 15. Gas–water production and pressure data of well A. (**a**) Gas–water production rate, and (**b**) bottomhole flow pressure.

The reservoir parameters, fluid parameters and fracturing parameters are shown in Table 7. Analysis of gas–water two-phase flow stage in well 8 are as shown in Figure 16.

Table 7. Values of basic parameters of well B.

Parameter	Value
Initial pressure, MPa	31.15
Initial gas saturation, decimal	0.6
Reservoir temperature, K	383.1
Reservoir thickness, m	10
Langmuir volume	1.96
Langmuir pressure, MPa	2200
Horizontal well length, m	1266
Number of fractures	19
Matrix porosity	0.064
Matrix Compressibility, MPa^{-1}	8×10^{-5}
Fracture Compressibility, MPa^{-1}	8×10^{-5}
Fracture width, m	0.5×10^{-2}

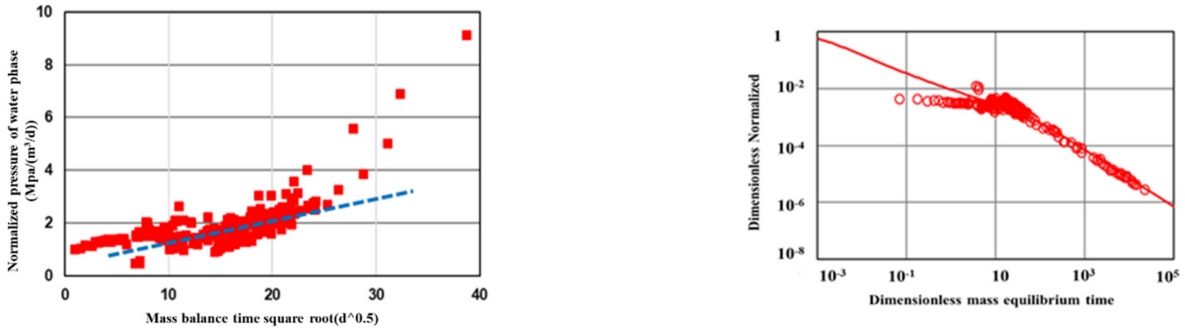


(**a**) Gas flow regime (**b**) Water flow regime

Figure 16. Analysis of gas–water two-phase flow stage in well 8. (**a**) Gas flow regime, and (**b**) water flow regime.

In the early production, the gas linear flow was long, and after 2 months the gas phase entered the fracture. For the water, it experiences fracture linear flow, and the water enters the boundary dominated flow and most fracturing fluid has been discharged. Thus, the fracture conductivity is high and the fracture half-length is small. The permeability of the SRV is large.

From Figure 17, the total length of the discrete fracture is 5152 m, and the stimulated reservoir volume is 233 × 10^4 m^3. The interpreted fracture network parameters are shown in Table 8.



(**a**) (**b**)

Figure 17. Production decline analysis of gas phase under gas–water two phases in well B. (**a**) Gas linear flow analysis, and (**b**) gas phase production data matching.

Table 8. Interpretation of fracture network parameters of well B.

Interpreted Parameters	Value
Fracture half-length (m)	82.1
Fracture permeability (mD)	685
Thickness of water invasion layer (m)	0.91
Permeability of water invasion (mD)	1.95×10^{-3}
SRV width (m)	45.3
SRV Permeability (mD)	3.12×10^{-3}

5. Conclusions

1. In this paper, a practical model considering gas adsorption of the shale matrix, water invasion layer and gas–water two-phase flow of hydraulic fracture is established, and the semi-analytical solution method is developed.
2. The new model is used to successfully analyze the production performance of the two modes of gas and water production. The two cases show different gas and water flow regimes:
   (1) The first production mode mainly shows three flow regimes, including water boundary dominated flow, gas linear flow and gas boundary dominated flow.
   (2) The second production mode mainly shows five flow stages, including water linear flow, water boundary dominated flow, gas bilinear flow, gas linear flow and gas boundary dominated flow.
3. The developed fracture parameters interpretation method can reasonably estimate the key parameters of the hydraulic fracture, water invasion layer and SRV of fracture well from the field example.

Author Contributions: Conceptualization, P.J. and L.N.; methodology, P.J.; software, Y.L.; validation, L.N., Y.L. and H.F.; formal analysis, P.J.; investigation, P.J. and L.N.; data curation, L.N. and Y.L.; writing—original draft preparation, L.N. and H.F.; writing—review and editing, P.J.; supervision, P.J.; project administration, P.J.; funding acquisition, P.J. All authors have read and agreed to the published version of the manuscript.

Funding: This research was partially funded by the National Natural Science Foundation of China (No. 52004307). We would further like to thank the financial support of the Science and technology project of CNPC-major project (No. ZLZX2020-02-04).

Data Availability Statement: Not applicable.

Conflicts of Interest: The authors declare no conflict of interest. The funders had no role in the design of the study; in the collection, analyses, or interpretation of data; in the writing of the manuscript; or in the decision to publish the results.

Appendix A

The flow equation of the SRV can be written as:

$$\frac{\partial}{\partial y}(-\rho_{sc} v_m) = 0.0864[\frac{\partial(\rho\phi_m)}{\partial t} + \frac{\partial V}{\partial t}] \tag{A1}$$

Introducing the gas isothermal adsorption equation:

$$V = \rho_{sc}\frac{V_L p_m}{p_L + p_m} \tag{A2}$$

Since the gas flow in SRV is regarded as an isothermal flow, dimensionless gas compression factor Z is introduced, and the gas phase isothermal compression coefficient is defined as:

$$c_g(p_m) = \frac{1}{p_m} - \frac{1}{z}\frac{dz}{dp_m} \tag{A3}$$

Gas density:

$$\rho_{sc} = \frac{pM}{zRT} \tag{A4}$$

Define the matrix compressibility as:

$$c_{pm} = \frac{1}{\phi_m}\frac{d\phi_m}{dp_m} \tag{A5}$$

Introduce the pseudo-pressure:

$$\psi_m(p_m) = 2\int_{p_i}^{p_m}\frac{p}{\mu_g z}dp \tag{A6}$$

Since gas flows isothermal in the SRV, the equation can be simplified to:

$$\frac{\partial^2\psi_m}{\partial x^2} = 0.0864\frac{\phi_m\mu(p_m)}{k_m}[c_{pm} + c_g(p_m) + \frac{z(p_m)p_{sc}T}{\phi_m z_{sc}T_{sc}}\frac{V_L p_L}{p_m(p_L+p_m)^2}]\frac{\partial\psi_m}{\partial t} \tag{A7}$$

where,

$$c_{tm}(p_m) = c_{pm} + c_g(p_m) + \frac{z(p_m)p_{sc}T}{\phi_m z_{sc}T_{sc}}\frac{V_L p_L}{p_m(p_L+p_m)^2} \tag{A8}$$

The last term in the above Equation (A8) represents the effect of desorption, so it is defined as the desorption compressibility C_d, the unit MPa^{-1}.

$$c_d(p_m) = \frac{z(p_m)p_{sc}T}{\phi_m z_{sc}T_{sc}}\frac{V_L p_L}{p_m(p_L+p_m)^2} \tag{A9}$$

Usually, an average formation pressure is adopted to replace the matrix pressure in the above equation, and take the average pressure as a constant value:

$$c_d = \frac{p_{sc}z(\overline{p}_m)TV_L p_L}{\phi_m z_{sc}T_{sc}\overline{p}_m(p_L+\overline{p}_m)^2} \tag{A10}$$

Therefore, the flow equation in the SRV is expressed as

$$\frac{\partial^2 \psi_m}{\partial y^2} = 0.0864 \frac{\phi_m \mu_g(p_m) c_{tm}(p_m)}{k_m} \frac{\partial \psi_m}{\partial t} \tag{A11}$$

Furthermore, for the nonlinear term on the right side of the equation, pseudo-time is used, which is defined as:

$$t_a = \int_0^t \frac{\mu_{gi} c_{tmi}}{\mu_g(\overline{p}_m) c_{tm}(\overline{p}_m)} dt \tag{A12}$$

Thus, the single-phase gas flow equation in the SRV is changed by use of pseudo-pressure and pseudo-time, and the flow equation can be obtained as follows:

$$\begin{cases} \frac{\partial^2 \psi_m}{\partial y^2} = \frac{\mu_{gi}(\phi c_t)_{mi}}{0.0864 k_m} \frac{\partial \psi_m}{\partial t_a} \\ \psi_m(y,t)|_{t_a=0} = \psi_i \\ \left.\frac{\partial \psi_m(y,t_a)}{\partial y}\right|_{y=L_F/2} = 0 \end{cases} \tag{A13}$$

The inner boundary of this region is coupled with the water invasion layer, and the pressure and flow rate on the inner boundary and the water invasion layer should be equal, respectively:

$$\psi_m|_{y=h_c+w_F/2} = \psi_c|_{y=h_c+w_F/2} \tag{A14}$$

Appendix B

Derivation of the flow equation of system in SRV. The solution of the model is obtained by using the Laplace transform.

For the SRV, the above equation is:

$$\frac{\partial^2 \overline{\psi}_{mD}}{\partial y_D^2} = \frac{s}{\eta_{mD}} \overline{\psi}_{mD} \tag{A15}$$

The general solution of Equation (A15) is:

$$\overline{\psi}_{mD} = A_2 \cosh\left[\sqrt{\frac{s}{\eta_{mD}}}(y_D - L_{FD}/2)\right] + B_2 \sinh\left[\sqrt{\frac{s}{\eta_{mD}}}(y_D - L_{FD}/2)\right] \tag{A16}$$

Substituting the initial and outer boundary conditions, B will be zero. Using the inner boundary conditions, we can obtain:

$$A_2 = \frac{\psi_{cD}(h_{cD} + w_{FD}/2)}{\cosh\left[\sqrt{\frac{s}{\eta_{mD}}}(h_{cD} + w_{FD}/2 - L_{FD}/2)\right]} \tag{A17}$$

Thus, the pressure solution in the SRV is:

$$\overline{\psi}_{mD}(y_D) = \psi_{cD}(h_{cD} + w_{FD}/2) \frac{\cosh\left[\sqrt{\frac{s}{\eta_{mD}}}(y_D - L_{FD}/2)\right]}{\cosh\left[\sqrt{\frac{s}{\eta_{mD}}}(h_{cD} + w_{FD}/2 - L_{FD}/2)\right]} \tag{A18}$$

Then, the flow between the SRV and the water invasion layer can be written as:

$$\begin{aligned} &\tfrac{k_m}{\mu}\tfrac{\partial \psi_{mD}}{\partial y_D}\Big|_{y_D=h_{cD}+w_{FD}/2} \\ &= \tfrac{k_m}{\mu}\psi_{cD}(h_{cD}+w_{FD}/2)\sqrt{\tfrac{s}{\eta_{mD}}}\tanh\left[\sqrt{\tfrac{s}{\eta_{mD}}}(h_{cD}+w_{FD}/2-L_{FD}/2)\right] \end{aligned} \tag{A19}$$

For the water invasion layer, the general solution of the flow model can be obtained as follows:

$$\overline{\psi}_{cD}(y_D) = A_1\cosh\left[\sqrt{\frac{s}{\hat{k}_{crg}\eta_{cD}}}(y_D-h_{cD}-w_{FD}/2)\right] + B_1\sinh\left[\sqrt{\frac{s}{\hat{k}_{crg}\eta_{cD}}}(y_D-h_{cD}-w_{FD}/2)\right] \tag{A20}$$

According to the boundary condition of the SRV, we have

$$\begin{aligned} B_1 &= \psi_{cD}(h_{cD}+w_{FD}/2)\tfrac{k_m}{k_c}\frac{\sqrt{s/\eta_{mD}}}{\sqrt{s/\left(\hat{k}_{crg}\eta_{cD}\right)}}\tanh\left[\sqrt{\tfrac{s}{\eta_{mD}}}(h_{cD}+w_{FD}/2-L_{FD}/2)\right] \\ &= \psi_{cD}(h_{cD}+w_{FD}/2)c_1(s) \end{aligned} \tag{A21}$$

Type,

$$c_1(s) = \frac{k_m}{k_c}\frac{\sqrt{s/\eta_{mD}}}{\sqrt{s/\left(\hat{k}_{crg}\eta_{cD}\right)}}\tanh\left[\sqrt{\frac{s}{\eta_{mD}}}(h_{cD}+w_{FD}/2-L_{FD}/2)\right] \tag{A22}$$

Then, the general solution of the flow model of the water invasion layer can be written as follows:

$$\overline{\psi}_{cD}(y_D) = \psi_{cD}(h_{cD}+w_{FD}/2)\left\{\begin{array}{c}\cosh\left[\sqrt{\frac{s}{\hat{k}_{crg}\eta_{cD}}}(y_D-h_{cD}-w_{FD}/2)\right] \\ +c_1(s)\sinh\left[\sqrt{\frac{s}{\hat{k}_{crg}\eta_{cD}}}(y_D-h_{cD}-w_{FD}/2)\right]\end{array}\right\} \tag{A23}$$

$$\begin{aligned} \psi_{cD}(h_{cD}+w_{FD}/2) &= \frac{\overline{\psi}_{FD}}{\cosh\left[\sqrt{\frac{s}{\hat{k}_{crg}\eta_{cD}}}(-h_{cD})\right]+c_1(s)\sinh\left[\sqrt{\frac{s}{\hat{k}_{crg}\eta_{cD}}}(-h_{cD})\right]} \\ &= \frac{\overline{\psi}_{FD}}{c_2(s)} \end{aligned} \tag{A24}$$

where,

$$c_2(s) = \cosh\left[\sqrt{\frac{s}{\hat{k}_{crg}\eta_{cD}}}(-h_{cD})\right] + c_1(s)\sinh\left[\sqrt{\frac{s}{\hat{k}_{crg}\eta_{cD}}}(-h_{cD})\right] \tag{A25}$$

Thus, the pressure solution of the water invasion layer is:

$$\overline{\psi}_{cD}(y_D) = \overline{\psi}_{FD}\frac{\cosh\left[\sqrt{\frac{s}{\hat{k}_{crg}\eta_{cD}}}(y_D-h_{cD}-w_{FD}/2)\right] + c_1(s)\sinh\left[\sqrt{\frac{s}{\hat{k}_{crg}\eta_{cD}}}(y_D-h_{cD}-w_{FD}/2)\right]}{c_2(s)} \tag{A26}$$

Then, the flow rate of water invasion layer into the hydraulic fracture is:

$$\tfrac{\partial \overline{\psi}_{cD}}{\partial y_D}\Big|_{y_D=w_{FD}/2} = \overline{\psi}_{FD}\sqrt{\frac{s}{\hat{k}_{crg}\eta_{cD}}}\frac{\sinh\left[\sqrt{\frac{s}{\hat{k}_{crg}\eta_{cD}}}(-h_{cD})\right]+c_1(s)\cosh\left[\sqrt{\frac{s}{\hat{k}_{crg}\eta_{cD}}}(-h_{cD})\right]}{c_2(s)} = \overline{\psi}_{FD}c_3(s) \tag{A27}$$

where,

$$c_3(s) = \sqrt{\frac{s}{\hat{k}_{crg}\eta_{cD}}}\frac{\sinh\left[\sqrt{\frac{s}{\hat{k}_{crg}\eta_{cD}}}(-h_{cD})\right] + c_1(s)\cosh\left[\sqrt{\frac{s}{\hat{k}_{crg}\eta_{cD}}}(-h_{cD})\right]}{c_2(s)} \tag{A28}$$

For the hydraulic fracture, it can be obtained by substituting the flow rate formula of water invasion layer to fracture

$$\frac{\partial^2\overline{\psi}_{FD}}{\partial x_D^2} + \frac{2\hat{k}_{crg}}{C_{FD}\hat{k}_{Frg}}\overline{\psi}_{FD}c_3(s) - \frac{s}{\hat{k}_{Frg}\eta_{FD}}\overline{\psi}_{FD} = 0 \tag{A29}$$

The above equation can be written as:

$$\frac{\partial^2\overline{\psi}_{FD}}{\partial x_D^2} - c_4(s)\overline{\psi}_{FD} = 0 \tag{A30}$$

$$c_4(s) = \frac{s}{\hat{k}_{Frg}\eta_{FD}} - \frac{2\hat{k}_{crg}}{C_{FD}\hat{k}_{Frg}}c_3(s) \tag{A31}$$

Similarly, the general solution of the hydraulic fracture flow model can be obtained as follows:

$$\overline{\psi}_{FD}(x_D) = A_F\cosh\left[\sqrt{c_4(s)}(x_D - x_{FD})\right] + B_F\sinh\left[\sqrt{c_4(s)}(x_D - x_{FD})\right] \tag{A32}$$

By using closed outer boundary condition, we find that B_F equals to zero. Additionally, A_F can be obtained by the use of constant pressure inner boundary condition

$$A_F = \frac{1 - S_c}{s}\frac{1}{\cosh\left[\sqrt{c_4(s)}(-x_{FD})\right]} \tag{A33}$$

Thus, the hydraulic fracture flow model is solved as follows:

$$\overline{\psi}_{FD}(x_D) = \frac{1 - S_c}{s}\frac{\cosh\left[\sqrt{c_4(s)}(x_D - x_{FD})\right]}{\cosh\left[\sqrt{c_4(s)}(-x_{FD})\right]} \tag{A34}$$

The gas production of the horizontal well through hydraulic fracture can be expressed as:

$$\overline{q}_{gD} = -\frac{\hat{k}_{Frg}k_{FD}w_{FD}}{\pi}\frac{\partial\overline{\psi}_{FD}}{\partial x_D}\bigg|_{x=0} \tag{A35}$$

Substituting the solution of the hydraulic fracture model, the solution of gas production is:

$$\overline{q}_{gD} = \frac{\hat{k}_{Frg}k_{FD}w_{FD}}{\pi}\frac{1 - S_c}{s}\sqrt{c_4(s)}\tanh\left(\sqrt{c_4(s)}\cdot x_{FD}\right) \tag{A36}$$

It should be noted that the gas production derived from analytical solution is in Laplace space, while the solution in real space needs to be obtained by a Stehfest numerical inversion algorithm.

Appendix C

Steps for solving the water phase flow equation. For the water invasion layer, the above equation can be changed into:

$$\frac{\partial^2 \overline{p}_{cD}}{\partial y_{cD}^2} = \frac{s}{\hat{k}_{crw}\eta_{cwD}} \frac{\partial \overline{p}_{cD}}{\partial t_D} \tag{A37}$$

The general solution of Equation (A38) is as follows.

$$\overline{p}_{cD} = A_1 \cosh\left[\sqrt{\frac{s}{\hat{k}_{crw}\eta_{cwD}}}(y_D - h_{cD} - w_{FD}/2)\right] + B_1 \sinh\left[\sqrt{\frac{s}{\hat{k}_{crw}\eta_{cwD}}}(y_D - h_{cD} - w_{FD}/2)\right] \tag{A38}$$

Substituting the initial and outer boundary conditions, we find that B equals to zero. By use of the inner boundary condition, we have

$$A_1 = \frac{\overline{p}_{FD}}{\cosh\left[\sqrt{\frac{s}{\hat{k}_{crw}\eta_{cwD}}}(-h_{cD})\right]} \tag{A39}$$

Thus, the pressure distribution of water invasion layer is

$$\overline{p}_{cD}(y_D) = \overline{p}_{FD} \frac{\cosh\left[\sqrt{\frac{s}{\hat{k}_{crw}\eta_{cwD}}}(y_D - h_{cD} - w_{FD}/2)\right]}{\cosh\left[\sqrt{\frac{s}{\hat{k}_{crw}\eta_{cwD}}}(-h_{cD})\right]} \tag{A40}$$

Further, the water flow from the water invasion layer to hydraulic fracture can be obtained as follows:

$$\left.\frac{\partial \overline{p}_{cD}}{\partial y_D}\right|_{y_D = w_{FD}/2} = \overline{p}_{FD}\sqrt{\frac{s}{\hat{k}_{crw}\eta_{cwD}}} \tanh\left[\sqrt{\frac{s}{\hat{k}_{crw}\eta_{cwD}}}(-h_{cD})\right] = \overline{p}_{FD} d_1(s) \tag{A41}$$

where,

$$d_1(s) = \sqrt{\frac{s}{\hat{k}_{crw}\eta_{cwD}}} \tanh\left[\sqrt{\frac{s}{\hat{k}_{crw}\eta_{cwD}}}(-h_{cD})\right] \tag{A42}$$

For the hydraulic fracture, the flow model becomes:

$$\frac{\partial^2 \overline{p}_{FD}}{\partial x_D^2} = \frac{s}{\hat{k}_{Frw}\eta_{FwD}} \overline{p}_{FD} - \frac{2\hat{k}_{crw}}{C_{FD}\hat{k}_{Frw}} \overline{p}_{FD} d_1(s) \tag{A43}$$

The above equation can be written as:

$$\frac{\partial^2 \overline{p}_{FD}}{\partial x_D^2} - d_2(s)\overline{p}_{FD} = 0 \tag{A44}$$

$$d_2(s) = \frac{s}{\hat{k}_{Frw}\eta_{FwD}} - \frac{2\hat{k}_{crw}}{C_{FD}\hat{k}_{Frw}} d_1(s) \tag{A45}$$

Similarly, the general solution of the flow model of the hydraulic fracture can be obtained as follows:

$$\overline{p}_{FD}(x_D) = A_F \cosh\left[\sqrt{d_2(s)}(x_D - x_{FD})\right] + B_F \sinh\left[\sqrt{d_2(s)}(x_D - x_{FD})\right] \tag{A46}$$

By use of a closed outer boundary, we find that B_F equals to zero. Additionally, by use of the constant pressure inner boundary condition, we have

$$A_F = \frac{1 - S_c}{s} \frac{1}{\cosh\left[\sqrt{d_2(s)}(-x_{FD})\right]} \tag{A47}$$

Thus, the solution of the flow model of the hydraulic fracture is as follows:

$$\overline{p}_{FD}(x_D) = \frac{1 - S_c}{s} \frac{\cosh\left[\sqrt{d_2(s)}(x_D - x_{FD})\right]}{\cosh\left[\sqrt{d_2(s)}(-x_{FD})\right]} \tag{A48}$$

The water production obtained is

$$\overline{q}_{wD} = -\frac{\hat{k}_{Frw} k_{FD} w_{FD}}{\pi} \frac{\partial \overline{p}_{FD}}{\partial x_D}\bigg|_{x_D=0} = \frac{\hat{k}_{Frw} k_{FD} w_{FD}}{\pi} \frac{1 - S_c}{s} \sqrt{d_2(s)} \tanh\left(\sqrt{d_2(s)} \cdot x_{FD}\right) \tag{A49}$$

References

1. Wattenbarger, R.; El-Banbi, A.; Villegas, M.; Maggard, J.B. Production analysis of linear flow into fractured tight gas wells. In Proceedings of the SPE Rocky Mountain Regional/Low-Permeability Reservoirs Symposium, Denver, CO, USA, 5–8 April 1998.
2. Bello, R.O.; Wattenbarger, R.A. Modelling and Analysis of Shale Gas Production with a Skin Effect. *J. Can. Pet. Technol.* **2010**, *49*, 37–48. [CrossRef]
3. Alahmadi, H.A.H.; Wattenbarger, R.A. Triple-porosity models: One further step towards capturing fractured reservoirs heterogeneity. In Proceedings of the SPE/DGS Saudi Arabia Section Technical Symposium and Exhibition, Al-Khobar, Saudi Arabia, 15–18 May 2011.
4. Brown, M.L.; Ozkan, E.; Raghavan, R.S.; Kazemi, H. Practical Solutions for Pressure-Transient Responses of Fractured Horizontal Wells in Unconventional Shale Reservoirs. *SPE Reserv. Eval. Eng.* **2009**, *14*, 663–676. [CrossRef]
5. Stalgorova, K.; Mattar, L. Analytical Model for Unconventional Multifractured Composite Systems. *SPE Reserv. Eval. Eng.* **2013**, *16*, 246–256. [CrossRef]
6. Shuang, A. Productivity Evaluation and Production Rule of Fractured Horizontal Wells in Shale Gas. Master's Thesis, China University of Petroleum, Beijing, China, 2015.
7. AlQuaimi, B.I.; Rossen, W.R. Capillary Desaturation Curve for Residual Nonwetting Phase in Natural Fractures. *SPE J.* **2018**, *23*, 788–802. [CrossRef]
8. Chen, Y.; Fu, L.; Hao, M. Derivation and application of gas adsorption equation and desorption equation. *China Offshore Oil Gas* **2018**, *30*, 85–89.
9. Stehfest, H. Numerical Estimation of Laplace Transforms. *ACM Commun.* **1970**, *13*, 47–49. [CrossRef]

Disclaimer/Publisher's Note: The statements, opinions and data contained in all publications are solely those of the individual author(s) and contributor(s) and not of MDPI and/or the editor(s). MDPI and/or the editor(s) disclaim responsibility for any injury to people or property resulting from any ideas, methods, instructions or products referred to in the content.